CHEMISTRY OF MATERIALS
Article

Chem. Mater. **2011,** *23,* 1023–1031 1023
DOI:10.1021/cm1030443

Multidirectional Hierarchical Nanocomposites Made by Carbon Nanotube Growth within Layer-by-Layer-Assembled Films

Jinjing Li,[†] Sudhanshu Srivastava,[‡] Jong G. Ok,[†] Yongyi Zhang,[†] Mostafa Bedewy,[†] Nicholas A. Kotov,*[,‡] and A. John Hart*[,†]

[†]*Mechanosynthesis Group, Department of Mechanical Engineering and* [‡]*Department of Chemical Engineering, University of Michigan, 2350 Hayward Street, Ann Arbor, Michigan 48109, United States*

Received October 22, 2010. Revised Manuscript Received December 13, 2010

We demonstrate fabrication of multidirectional and hierarchical carbon nanotube (CNT) films on diverse substrates, using nanocomposite catalyst films prepared by layer-by-layer (LBL) assembly. CNT density and yield are controlled by the thickness of a montmorillonite clay/poly(dyallyldimethyl ammonium chloride (MTM/PDDA) support film. Using identical methods, few-walled CNTs are grown on flat silicon substrates, carbon fibers, and titanium wire mesh. On flat substrates, unique bilayer CNT forests, reminiscent of microscale "accordions", form because of diffusion of the Fe catalyst through the support which is then split because of mechanical forces exerted by the growing CNTs. Electrochemical measurements of CNT-coated Ti wires demonstrate an 85-fold enhancement in specific capacitance, and 7.1 F/g for the CNTs alone. This novel approach to substrate engineering for CNT growth can create materials with unique and nonlinear properties by hierarchical ordering of CNTs at multiple length scales, and is scalable to large-area foils and fabrics.

Introduction

The outstanding properties[1] of carbon nanotubes (CNTs) have generated wide interest and progress in their controlled production. Practical use[2,3] of CNTs requires control of their key nanoscale characteristics such as diameter, packing, and alignment, as well as their collective order and arrangement at higher length scales. It is especially important to incorporate CNTs in composite architectures with other materials to achieve complementary and multidirectional properties owing to hierarchical control of CNT organization. Such hybrid CNT materials with unique structural features suggest a foundation for major improvements in the performance of, for example, battery and capacitor electrodes, transparent conductors, static discharge films, filtration membranes, electromechanical probes, thermal interfaces, composite sports equipment, and next-generation biointerfaces.[3−7] Overall, development of scalable three-dimensional composite architectures is a long-standing challenge that has stimulated many innovations in fiber processing and weaving,[8] and now demands new methods of bottom-up organization of nanostructures that can impart new passive and active functions in materials.[9,10]

For these needs, it is particularly advantageous to fabricate CNTs by chemical vapor deposition (CVD), since CVD affords local control along with scalability to large areas and volumes. While bulk production of CNT powders by CVD has become a relatively mature technology, direct growth of CNTs on substrates is vital for achieving the highly organized architectures needed for composites.[4] Specifically, the diameter, density, and orientation of CNTs within films have important effects on the collective properties of the assembly, and integration of CNTs on more complex substrates such as advanced fibers and metal foils is needed for use of CNTs in applications such as structural composites[11,12] and electrochemical storage devices.[13]

*To whom correspondence should be addressed. E-mail: kotov@umich.edu (N.A.K.), ajohnh@umich.edu (A.J.H.).

(1) Harris, P. J. F. *Carbon Nanotube Science - Synthesis, Properties, and Applications*; Cambridge University Press: New York, 2009.
(2) Baughman, R. H.; Zakhidov, A. A.; de Heer, W. A. *Science* **2002**, *297*(5582), 787–792.
(3) Endo, M.; Hayashi, T.; Kim, Y. A.; Terrones, M.; Dresselhaus, M. S. *Philos. Trans. R. Soc., A* **2004**, *362*(1823), 2223–2238.
(4) Eklund, P. C.; Ajayan, P. M.; Blackmon, R.; Hart, A. J.; Kong, J.; Pradhan, B.; Rao, A.; Rinzler, A. *International Assessment of Research and Development on Carbon Nanotubes: Manufacturing and Applications*; World Technology Evaluation Center, Inc.: Baltimore, MD, 2007.
(5) Holt, J. K.; Park, H. G.; Wang, Y. M.; Stadermann, M.; Artyukhin, A. B.; Grigoropoulos, C. P.; Noy, A.; Bakajin, O. *Science* **2006**, *312*(5776), 1034–1037.
(6) Wu, Z.; Chen, Z.; Du, X.; Logan, J. M.; Sippel, J.; Nikolou, M.; Kamaras, K.; Reynolds, J. R.; Tanner, D. B.; Hebard, A. F.; Rinzler, A. G. *Science* **2004**, *305*(5688), 1273–1276.
(7) Kotov, N. A.; Winter, J. O.; Clements, I. P.; Jan, E.; Timko, B. P.; Campidelli, S.; Pathak, S.; Mazzatenta, A.; Lieber, C. M.; Prato, M.; Bellamkonda, R. V.; Silva, G. A.; Kam, N. W. S.; Patolsky, F.; Ballerini, L. *Adv. Mater.* **2009**, *21*(40), 3970–4004.
(8) Dickinson, L. C.; Farley, G. L.; Hinders, M. K. *J. Compos. Technol. Res.* **1999**, *21*(1), 3–15.
(9) Sanchez, C.; Julian, B.; Belleville, P.; Popall, M. *J. Mater. Chem.* **2005**, *15*(35−36), 3559–3592.
(10) Chou, T. W.; Gao, L. M.; Thostenson, E. T.; Zhang, Z. G.; Byun, J. H. *Compos. Sci. Technol.* **2010**, *70*(1), 1–19.
(11) Qian, H.; Greenhalgh, E. S.; Shaffer, M. S. P.; Bismarck, A. *J. Mater. Chem.* **2010**, *20*(23), 4751–4762.
(12) Coleman, J. N.; Khan, U.; Gun'ko, Y. K. *Adv. Mater.* **2006**, *18*(6), 689–706.
(13) Su, D. S.; Schlogl, R. *ChemSusChem* **2010**, *3*(2), 136–168.

Published on Web 01/05/2011

While there have been many recent developments in CNT synthesis toward these goals,[14−17] the viability of a particular synthesis method (and specifically the combination of catalyst and substrate) is typically restricted to a narrow window of process conditions (i.e., temperatures, feedstocks) and CNT characteristics (i.e., film organization, diameter, density). In other words, the characteristics of the CNT film are coupled intimately with the growth process parameters and the characteristics of the substrate. For example, efficient CNT growth typically requires a transition metal oxide support (e.g., Al_2O_3) that enhances growth because of electron transfer to the catalyst, and prevents agglomeration of the catalyst particles.[18,19] This often restricts efficient CNT growth to flat substrates such as silicon wafers that can be coated with thin oxide layers, and hence limits structural control of the produced materials. The support and catalyst are typically deposited by physical vapor deposition (PVD) methods, which generally require a high vacuum environment.[20−22] As a result, growth of CNTs on topographically complex three-dimensional (3D) substrates usually requires choice of a substrate that already contains the catalyst,[23,24] or requires multistep coating.[25,26] Further, while wet chemical methods can create nanoparticle catalysts for growth of CNTs and other one-dimensional nanostructures, uniform coating of 3D substrates using wet chemical methods is difficult as well. Low-cost methods of catalyst preparation on diverse substrates, along with the ability to control the key characteristics of CNT films via straightforward and scalable means, are therefore needed for large-scale production of CNT films with complex and hierarchical order.

We present a new and versatile method of preparing substrates for CNT film growth, where the catalyst is prepared as a metal-ceramic nanocomposite using layer-by-layer (LBL) assembly. In contrast to physical deposition methods, the nanocomposite catalyst (Fe/MTM) is deposited at room temperature and pressure, by a simple dip-coating LBL assembly method. LBL has been widely used to assemble complex films from modular nanoscale components,[27,28] and has been used to deposit catalyst particles for CNT growth;[29] however, the utility of previous work was limited because it did not deposit a growth-promoting support layer as well. Similar material combinations were used to grow CNTs from catalyst-coated porous wollastonites,[30] flake[31] or lamellar[32] substrates, such as by injection CVD of aerosols containing both the catalyst-coated substrate material and the carbon source.[33] Nevertheless, these bulk exfoliation approaches did not exploit the ability of nanocomposite catalysts to control CNT film architecture on substrates.

LBL deposition of the both support and catalyst as a robust nanocomposite layer facilitates control of the morphology and thickness of CNT films, and enables conformal CNT growth on complex substrates such as metal foils and carbon fibers. This versatile solution-based technique overcomes limitations of physical vapor deposition, which typically require expensive equipment and high vacuum conditions. Further, the nanocomposite LBL catalyst enables large-scale growth of CNT films with controlled hierarchy, without requiring changes of the catalyst system. This is engineered by competition between the formation of the nanocomposite catalyst by diffusion and the forces involved in self-organization of the CNT film, to create, for example, self-stratified CNT bilayers. Our method can potentially enable hierarchical ordering of CNTs at multiple length scales, and may find use in designing materials with nonlinear mechanical properties[34] or other metamaterial characteristics.[35]

Experimental Methods

Materials. Na^+-Montmorillonite ("Cloisite Na^+", MTM) powder was purchased from Southern Clay Products (Gonzales, TX). Poly(dyallyldimethyl ammonium chloride) (PDDA) was purchased from Sigma-Aldrich. MTM and PDDA were both dispersed in E-pure water (Barnstead). Fe_2O_3 nanoparticles were synthesized from $FeCl_2$, $FeCl_3$, and NH_4OH (Sigma-Aldrich) via a previously published procedure,[36] with mean diameter 10−12 nm.

LBL Film Preparation. The nanocomposite catalyst consisted of a desired number of Montmorillonite (MTM) clay layers beneath a layer of magnetite (citrate-functionalized Fe_2O_3) nanoparticles, which were assembled by LBL using positively charged PDDA.

(14) Talapatra, S.; Kar, S.; Pal, S. K.; Vajtai, R.; Ci, L.; Victor, P.; Shaijumon, M. M.; Kaur, S.; Nalamasu, O.; Ajayan, P. M. *Nat. Nanotechnol.* **2006**, *1*(2), 112–116.
(15) Yamamoto, N.; Hart, A. J.; Garcia, E. J.; Wicks, S. S.; Duong, H. M.; Slocum, A. H.; Wardle, B. L. *Carbon* **2009**, *47*(3), 551–560.
(16) Nessim, G. D.; Seita, M.; O'Brien, K. P.; Hart, A. J.; Bonaparte, R. K.; Mitchell, R. R.; Thompson, C. V. *Nano Lett.* **2009**, *9*(10), 3398–3405.
(17) Hata, K.; Futaba, D. N.; Mizuno, K.; Namai, T.; Yumura, M.; Iijima, S. *Science* **2004**, *306*(5700), 1362–1364.
(18) Ago, H.; Nakamura, K.; Uehara, N.; Tsuji, M. *J. Phys. Chem. B* **2004**, *108*(49), 18908–18915.
(19) Wang, Y. Y.; Luo, Z. Q.; Li, B.; Ho, P. S.; Yao, Z.; Shi, L.; Bryan, E. N.; Nemanich, R. J. *J. Appl. Phys.* **2007**, *101*, 124310.
(20) Sinnott, S. B.; Andrews, R.; Qian, D.; Rao, A. M.; Mao, Z.; Dickey, E. C.; Derbyshire, F. *Chem. Phys. Lett.* **1999**, *315*(1−2), 25–30.
(21) Hart, A. J.; Slocum, A. H.; Royer, L. *Carbon* **2006**, *44*(2), 348–359.
(22) Minea, T. M.; Point, S.; Gohier, A.; Granier, A.; Godon, C.; Alvarez, F. *Surf. Coat. Technol.* **2005**, *200*(1−4), 1101–1105.
(23) Karwa, M.; Iqbal, Z.; Mitra, S. *Carbon* **2006**, *44*(7), 1235–1242.
(24) Karwa, M.; Iqbal, Z.; Mitra, S. *J. Mater. Chem.* **2006**, *16*(28), 2890–2895.
(25) Huang, S. M.; Mau, A. W. H. *J. Phys. Chem. B* **2003**, *107*(33), 8285–8288.
(26) Huang, S. M. *Chem. Phys. Lett.* **2003**, *374*(1−2), 157–163.
(27) Podsiadlo, P.; Kaushik, A. K.; Arruda, E. M.; Waas, A. M.; Shim, B. S.; Xu, J. D.; Nandivada, H.; Pumplin, B. G.; Lahann, J.; Ramamoorthy, A.; Kotov, N. A. *Science* **2007**, *318*(5847), 80–83.
(28) Srivastava, S.; Kotov, N. A. *Acc. Chem. Res.* **2008**, *41*(12), 1831–1841.
(29) Liu, J. W.; Li, X. J.; Schrand, A.; Ohashi, T.; Dai, L. M. *Chem. Mater.* **2005**, *17*(26), 6599–6604.
(30) Zhao, M. Q.; Zhang, Q.; Huang, J. Q.; Nie, J. Q.; Wei, F. *ChemSusChem* **2010**, *3*(4), 453–459.
(31) Zhao, M. Q.; Zhang, Q.; Jia, X. L.; Huang, J. Q.; Zhang, Y. H.; Wei, F. *Adv. Funct. Mater.* **2010**, *20*(4), 677–685.
(32) Zhang, Q.; Zhao, M. Q.; Huang, J. Q.; Liu, Y.; Wang, Y.; Qian, W. Z.; Wei, F. *Carbon* **2009**, *47*(11), 2600–2610.
(33) Pinault, M.; Pichot, V.; Khodja, H.; Launois, P.; Reynaud, C.; Mayne-L'Hermite, M. *Nano Lett.* **2005**, *5*(12), 2394–2398.
(34) Bertoldi, K.; Reis, P. M.; Willshaw, S.; Mullin, T. *Adv. Mater.* **2010**, *22*(3), 361.
(35) Smith, D. R.; Pendry, J. B.; Wiltshire, M. C. K. *Science* **2004**, *305*(5685), 788–792.
(36) Sheparovych, R.; Sahoo, Y.; Motornov, M.; Wang, S. M.; Luo, H.; Prasad, P. N.; Sokolov, I.; Minko, S. *Chem. Mater.* **2006**, *18*(3), 591–593.

Prior to the LBL assembly of the MTM/PDDA film,[27] the Si wafers were cleaned with piranha solution (3:1 H_2SO_4/H_2O_2), for 1 h, followed by thorough rinsing with deionized water. For the LBL assembly, the clean Si wafer was immersed in 1 wt % solution of PDDA (mass: $1 \times 10^5 - 2 \times 10^5$ g-mol^{-1}), for 2 min, rinsed with DI water for 1 min, then immersed in 0.5 wt % MTM dispersion for 2 min, then rinsed again for 1 min. The cycle was then repeated as necessary to obtain the 10, 20, 30, 40, and 50 bilayers of PDDA and MTM. Once the desired number of bilayers was prepared, the corresponding films were annealed (see below) to remove the PDDA from among the MTM layers. After annealing, the samples were immersed in PDDA again for 10 min at ambient temperature and then rinsed with DI water for 2 min, as described in our previous work.[37,38] PDDA facilitated adsorption of the catalyst nanoparticles in the final step. Accordingly, the films were then dipped in a solution of negatively charged Fe_2O_3 nanoparticles[36] ($\approx$10−12 nm in diameter, ~10 mg/mL) for 10 min and then rinsed again with DI water for 2 min. The films were then again annealed to remove the PDDA, and to create the final nanocomposite catalyst. The nanocomposite catalysts were also deposited onto aerospace-grade carbon fibers (provided by the Boeing Company) and titanium wire mesh (0.076 mm diameter wire, #40918 from Alfa Aesar) via the same process.

Annealing. The substrates were annealed after deposition of MTM, PDDA, and Fe_2O_3 nanoparticle films. The Si wafer samples were loaded into the center of the quartz tube furnace (see below), and then baked in air at 825 °C for 30 to 35 min, with the ends of the quartz tube open. The Ti mesh samples were annealed at 825 °C in a continuous air flow of 100 sccm (Airgas, zero grade) for 30 min. Carbon fiber samples were annealed at 500 °C in a continuous air flow of 100 sccm (Airgas, zero grade) for 60 min. The lower annealing temperature of the carbon fiber was necessary to prevent damage to the material due to oxidation.

CNT Growth. CNT growth was performed in a single-zone atmospheric pressure quartz tube furnace (Lindberg) with a 30 cm long heating zone, loading a quartz tube (inside diameter 22 mm), using flows of He (99.999%, Airgas), C_2H_4 (99.5%, Airgas), and H_2 (99.999%, Airgas). A bubbler filled with ethanol (C_2H_5OH) was added to the gas delivery system, so that part of the He flow could be diverted through the bubbler, therefore adding a small concentration of ethanol vapor to the growth atmosphere.[39] The annealed growth substrates were cut into 5 × 10 mm pieces, and placed on a 1 × 6 cm section of Si wafer as a sample holder. The sample holder was initially placed outside the heated region of the furnace. The quartz tube was flushed for 5 min with 1000 sccm He, and then the furnace was ramped up from room temperature to 825 °C in 10 min under a flow of 400 sccm H_2 and 100 sccm He. The temperature was then held at 825 °C for 25 min under gas flows of 400 sccm H_2, 100 sccm He, and 100 sccm C_2H_4. At the desired times, 50 sccm He was diverted through the bubbler. After ethanol had been introduced for 5 min, the sample holder was rapidly moved into the heated region using a steel pushrod that was fed through a fitting in the furnace end-cap. After the desired growth time elapsed, the furnace power was turned off, the furnace cover was opened, and the samples were cooled in 1000 sccm He flow for 10 min. Carbon fiber samples were cut into 5 mm bundles and Ti mesh samples were cut into 15 mm by 15 mm pieces, and both followed the same growth recipe as the Si wafer samples.

Characterization. Substrates were characterized by scanning electron microscopy (SEM) using a Philips XL30-FEG-SEM (10 keV, and spot size 3), transmission electron microscopy (TEM) using 300 keV, thermo gravimetric analysis (TGA, Perkin-Elmer Pyris 1). TGA samples were prepared by removing ≈0.5 mg of CNTs grown with 40 support bilayers using a razor blade. The sample was first held at 30 °C for 30 min, and then heated to 900 °C in air (10 °C/min).

Small-angle X-ray scattering (SAXS) was also used to quantify the CNT alignment for samples grown from the nanocomposite catalyst. Alignment was quantified by calculating the Hermans orientation parameter, which is a measure for the mean square cosine of the angle between the average CNT direction and a reference direction. X-ray scattering data are used to obtain this mean square cosine by numerical integration of the corresponding intensity distribution about the beam's axis.[40] This technique was first developed for characterizing the alignment of polymer chains[41] and was later adopted for mapping the morphology of CNTs within an array.[42,43] SAXS was carried out at the G1 station at the Cornell High Energy Synchrotron Source (CHESS), using a synchrotron X-ray beam energy of 10 ± 0.1 keV. To focus the beam size to ≈10 μm, a single-bounce monocapillary was used, and the samples were placed on a motorized stage at the focal length of the focusing optics.[44]

Cyclic voltammetry (CV) tests were performed using a potentiostat (Epsilon, Bioanalytical Systems Inc. Data was recorded by BASi-Epsilon-EC, Ver 1.60.70_XP). The CNT-coated Ti mesh (or control substrate) was used as the working electrode, AgCl/Ag was the reference electrode, and Au foil was the counter electrode. The electrolyte was 80 mL of NaOH-K_3PO_4-EDTA buffer solution (Buffer solution concentrate, SB109−500, Fisherchemicals, 1:24 dilute), which maintained pH = 7.00 ± 0.02. CV tests were carried out at a scan rate of 100 mV/s, and a voltage sweep range from −500 to 500 mV, for 10 cycles. The capacitance was calculated using the last cycle of data.

Results and Discussion

CNT Growth Control and Self-Stratification on Flat Substrates. The step-by-step process for preparing the nanocomposite catalysts by LBL assembly and for CNT growth is shown in Figure 1, and full details are written in the Experimental Methods section. In brief, the process has five steps: (1) deposition of the MTM support by the LBL method; (2) removal of the polymer between the MTM layers by annealing in air; (3) deposition of the Fe catalyst on top of the annealed MTM film; (4) a second annealing process to create the nanocomposite catalyst; and (5) CNT growth in a hydrocarbon atmosphere, which is a mixture of $C_2H_5OH/C_2H_4/H_2$/He. After a systematic search of the CNT growth parameter space, we found a

(37) Mamedov, A. A.; Kotov, N. A. *Langmuir* **2000**, *16*(13), 5530–5533.
(38) Mamedov, A.; Ostrander, J.; Aliev, F.; Kotov, N. A. *Langmuir* **2000**, *16*(8), 3941–3949.
(39) Zhang, Y.; Gregoire, J. M.; van Dover, R. B.; Hart, A. J., submitted for publication **2009**.
(40) Alexander, L. E. *X-ray diffraction methods in polymer science*; Wiley-Interscience: New York, 1969; p xv, 582.
(41) Hermans, P. H. *Contribution to the physics of cellulose fibres; a study in sorption, density, refractive power and orientation*; Elsevier Pub. Co.: Amsterdam, The Netherlands, 1946; p xvi, 221.
(42) Wang, B. N.; Bennett, R. D.; Verploegen, E.; Hart, A. J.; Cohen, R. E. *J. Phys. Chem. C* **2007**, *111*(48), 17933–17940.
(43) Wang, B. N.; Bennett, R. D.; Verploegen, E.; Hart, A. J.; Cohen, R. E. *J. Phys. Chem. C* **2007**, *111*(16), 5859–5865.
(44) Meshot, E.; Bedewy, M.; Lyons, K.; Woll, A.; Juggernauth, K.; Tawfick, S.; Hart, A. *Nanoscale* **2010**, *2*(6), 896–900.

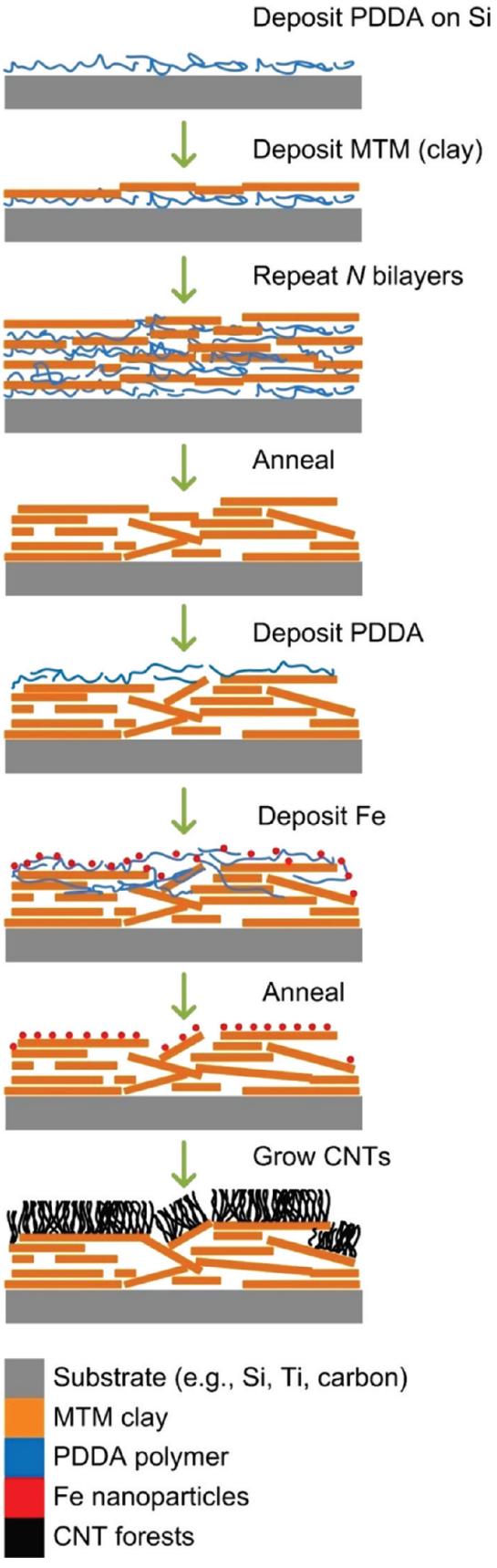

Figure 1. Scheme for deposition of supported catalyst by LBL assembly, followed by CNT growth by atmospheric pressure CVD.

set of process parameters (see Experimental Methods section) that maximized the CNT forest height for the formulations of the nanocomposite catalyst that we studied. The data in this paper were obtained at these conditions.

We first discuss CNT growth from nanocomposite Fe/MTM catalysts deposited on flat silicon substrates. We found that the thickness of the MTM support, which is precisely determined by the number of layers (N) deposited by LBL, provides a facile means of tuning the morphology and yield (growth height) of the CNTs. Figure 2a shows the relationship between the CNT film thickness and the number of MTM bilayers. This profound trend in CNT film thickness, which increases for $N = 10-40$ and subsequently decreases for $N = 50-100$ indicates that the thickness of the MTM support film controls the behavior the Fe catalyst particles for CNT growth. This is known because the conditions of Fe particle deposition were the same in all cases, and the mechanism for this is discussed later.

SEM examination reveals that, with increasing N, the CNT film first transitions from a tangled morphology (Figure 2d) to a vertically aligned morphology (Figure 2e). When there is a sufficient density of active catalyst particles on the substrate, the CNTs self-organize into the vertically aligned forest at the start of the growth process. After this condition is satisfied, the CNTs can grow to very high aspect ratios (length/diameter $\gg$1000) while collectively maintaining the aligned film texture. On the other hand, when the density of CNT growth is below the critical threshold[45] for vertical alignment, the terminal height of the CNT forest is much lower because the entanglement among the CNTs causes significant steric hindrance. At $N = 40$, the CNT film height reaches a maximum and is uniquely self-stratified into two vertically aligned layers as discussed later; and for $N > 40$ the CNT film height decreases monotonically with increasing N (Figure 2f). Sparse tangled CNTs and amorphous carbon deposits were observed after growth experiments with Fe particles deposited by LBL on bare thermally oxidized Si wafers without MTM. Therefore, the MTM is essential to physically stabilize the Fe particles, and promotes the catalytic activity of Fe for efficient CNT growth. This role is consistent with many previous studies of how metal oxides, especially Al_2O_3, promote high-yield CNT growth from Fe.[17,21,46] From previous work, we estimate the thickness of one bilayer (MTM/PDDA) to be approximately 20 nm.[47] However, annealing removes the PDDA, so the final thickness after annealing is closer to the MTM layer thickness of 0.94 nm.

TEM images (Figure 2b) show that the CNTs are typically multiwalled under these growth conditions, with average outer diameter 7.0 ± 1.7 nm, and 4.3 ± 1.1 walls. It should be possible to control the CNT diameter by using different sized nanoparticles, in conjunction with

(45) Bedewy, M.; Meshot, E. R.; Guo, H. C.; Verploegen, E. A.; Lu, W.; Hart, A. J. *J. Phys. Chem. C* **2009**, *113*(48), 20576–20582.
(46) Amama, P. B.; Pint, C. L.; Kim, S. M.; McJilton, L.; Eyink, K. G.; Stach, E. A.; Hauge, R. H.; Maruyama, B. *ACS Nano* **2010**, *4*(2), 895–904.
(47) Tang, Z. Y.; Kotov, N. A.; Magonov, S.; Ozturk, B. *Nat. Mater.* **2003**, *2*(6), 413–U8.

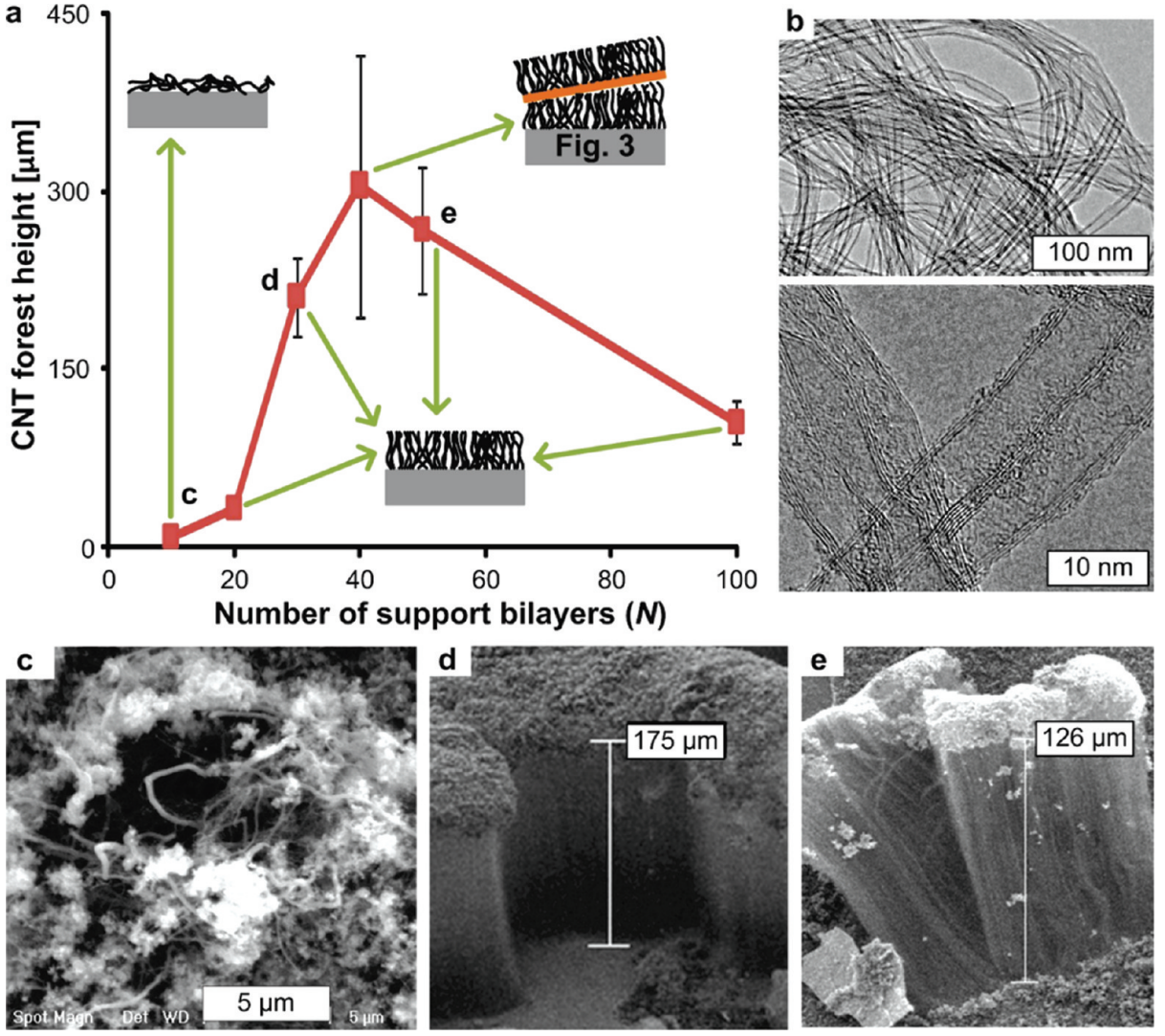

Figure 2. Effect of the number of MTM support layers and CNT forest morphology and height: (a) relationship between number of layers and CNT height after 20 min exposure to the reaction atmosphere. The error bars in (a) indicate ±1 standard deviation of the height measured at several locations on the substrate; (b) TEM image of individual CNTs separated from a film grown on a substrate with 40 support layers; (c−e) SEM images of CNT films on substrates with 10, 40, and 50 bilayers, respectively.

the appropriate CNT growth conditions (e.g., pressure, temperature, feedstock mixture).

The purity and structural quality of the CNTs grown from 40 support layers were evaluated by TGA, and these results are shown in the Supporting Information, Figure S1. The TGA curves of mass versus temperature reveal three important points: (1) a mass loss of less than 5% below 500 °C, indicating that the sample contains less than 5% amorphous carbon; (2) a derivative peak at ≈720 °C, indicating that the structural quality of the CNTs is comparable to CNT forests grown from physically deposited catalyst thin films;[48] and (3) a residual mass of ≈25%, indicating ≈300% yield of CNTs per unit mass of MTM support.

The inhomogeneity in the texture of the LBL-deposited films, which arises because of the finite size and flexibility of the MTM flakes, leads to non-uniformity in the CNT forests. Further, the local topography of the MTM support can affect the local organization of the CNTs and hence cause local variations in the film thickness. When this variation is substantial, the resulting mechanical stress[49,50] that arises during CNT growth causes the CNT film to separate into distinct pillars which may grow at different rates. Many of the films made from the nanocomposite catalyst exhibit this morphology, and therefore the CNT film height was calculated by averaging several measurements taken over a large area. The roughness of the nanocomposite catalyst can, in principle, be controlled by the LBL deposition conditions, and this can be a means of controlling the accessible surface area of the CNT films.

The morphology and thickness of the MTM support also affect how the Fe_2O_3 particles are incorporated into the MTM, and how the nanocomposite catalyst forms during the annealing step that follows Fe_2O_3 deposition. These behaviors in turn affect the morphology and

(48) Meshot, E. R.; Plata, D. L.; Tawfick, S.; Zhang, Y. Y.; Verploegen, E. A.; Hart, A. J. *ACS Nano* **2009**, *3*(9), 2477–2486.
(49) Han, J. H.; Graff, R. A.; Welch, B.; Marsh, C. P.; Franks, R.; Strano, M. S. *ACS Nano* **2008**, *2*(1), 53–60.
(50) Hart, A. J.; Slocum, A. H. *Nano Lett.* **2006**, *6*(6), 1254–1260.

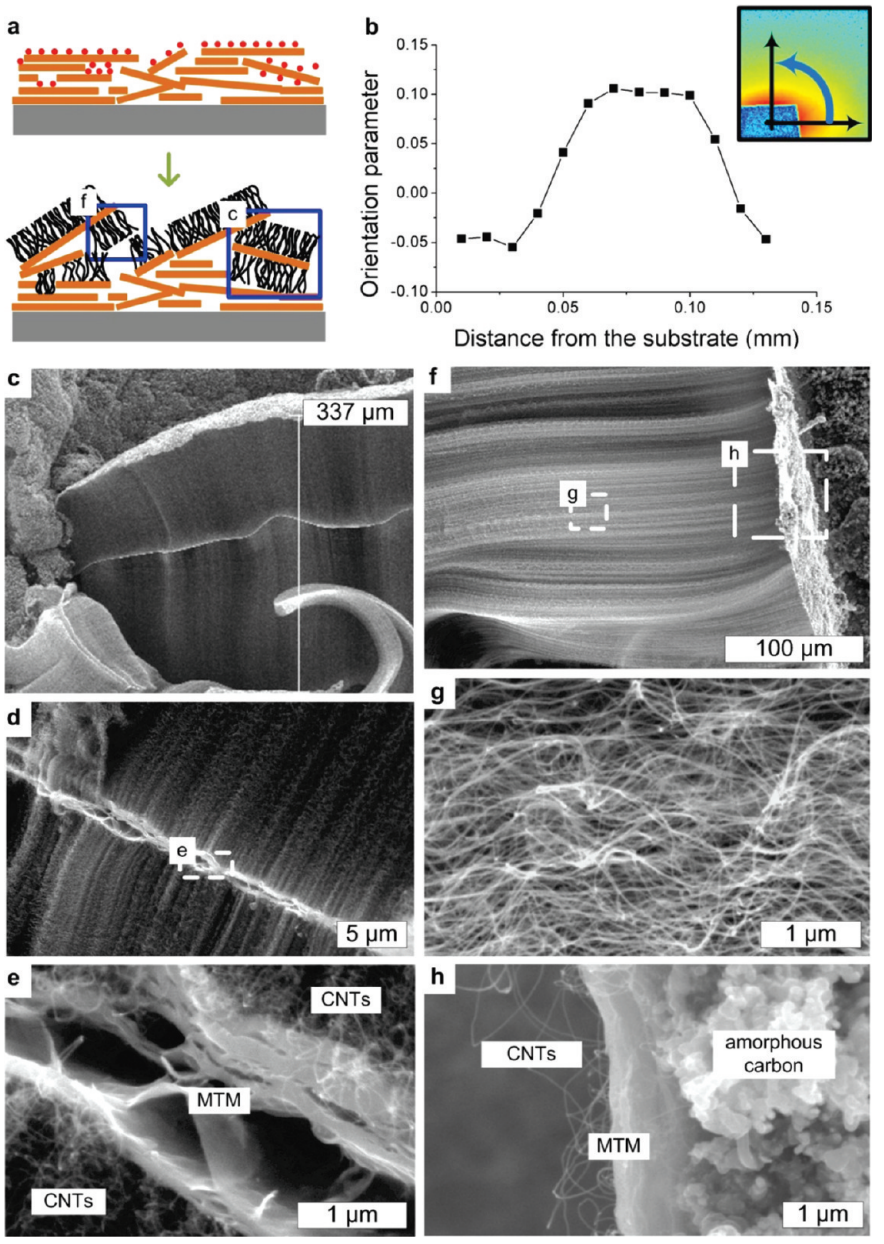

Figure 3. Self-stratified CNT films growth with 40 support bilayers: (a) schematic of self-stratified growth mechanism by Fe migration through the support layers, followed by mechanical cleavage because of forces exerted during the initial stages of CNT growth; (b) map of Hermans orientation parameter, indicating multidirectional texture at top and bottom of film; (c−e) SEM images of bidirectional CNT forest growth from separated nanocomposite film; (f−h) SEM images of unidirectional CNT forest growth from separated nanocomposite film.

thickness of the CNT film. Although the MTM comprises sheets with in-plane dimensions that far exceed their nanoscale thickness, we have previously shown that polymers can diffuse through the nanoscale gaps among the MTM sheets.[51] This occurs during Fe_2O_3 deposition as well; thus there are catalyst particles not only on the top surface of the MTM support film, but also between the MTM layers beneath the surface.

The migration of Fe into the MTM support, and the extrusive forces generated by the nucleation and growth of CNTs, lead to the unique self-stratified CNT forests shown in Figure 3. The CNTs separate the nanocomposite catalyst structure into multiple layers, and CNTs grow from the faces of the separated layers. In different areas of the same sample, we observed bidirectional growth of aligned CNTs from stratified layers in the midsection of the forest (Figure 3c−e), and unidirectional growth from layers that separate from the substrate and remain at the top of the growing forest (Figure 3f−h). The self-stratification confirms that the catalyst is a true nanocomposite, and the self-organization of CNTs growing from Fe particles beneath the top surface causes the composite to swell, and causes the layer to separate. The high in-plane aspect ratio of the stratified catalyst layers profits from the robust mechanical properties and high thermal stability of the MTM layers.[27,52] Nevertheless, further study of the strength of CNT-MTM adhesion and CNT-substrate adhesion is needed.

(51) Podsiadlo, P.; Michel, M.; Lee, J.; Verploegen, E.; Kam, N. W. S.; Ball, V.; Qi, Y.; Hart, A. J.; Hammond, P. T.; Kotov, N. A. *Nano Lett.* **2008**, *8*(6), 1762–1770.

The morphology of the CNT ensembles was also investigated by spatially resolved measurement of the CNT alignment from SAXS patterns. We mapped the Hermans orientation parameter with 10 μm spatial resolution along the height of the CNT films.[44] The results for a multilayer CNT forest (40 bilayers) are shown Figure 3b, revealing that the preferential vertical alignment of CNTs is greatest in the middle portion of the film height, and the alignment decays at the top and bottom of the film. This behavior is in agreement with previous results obtained for CNT growth on catalysts prepared by e-beam evaporation,[53] which were used to elucidate the successive stages of growth and termination of CNTs based on a collective mechanism.[45] Nevertheless, the small values of the orientation parameter throughout the LBL samples indicate that the CNTs are generally more tortuous than forests grown from thin-film catalysts in our previous work. In addition, the separation and stratification of the CNTs observed in LBL samples gives rise to a multidirectional texture, that is, the scattering pattern obtained on the X-ray area detector represents an image of the collective scattering of all CNTs in the beam path. Despite the local alignment among CNTs within a bundle, the global tilt angles of these bundles (separate ensembles) could be different in different locations of the same sample, as shown in SEM images in Supporting Information, Figure S2, thus causing the measured orientation values to represent a case of a more random orientation. This population may even include some horizontally oriented CNTs, especially at the bottom of the CNT forest (near the substrate), where negative values of the orientation parameter were measured.

Bilayer CNT forests were observed only on substrates prepared with 40 MTM layers, and substrates with more than 40 (up to 100) layers showed single-layer CNT forests. This result confirms the competition between Fe migration inside the MTM, and the process of self-organization that is needed to create an aligned forest. When the MTM support is thicker (more layers) and the amount of Fe deposited is kept the same, the Fe spreads out farther into the MTM, and therefore there is an insufficient local density of catalyst to self-organize and produce enough force to stratify the nanocomposite into multiple catalyst films. On the other hand, when the support is thinner than 40 layers, there are only enough catalyst particles to self-organize a forest on the top surface of the film. The relative surface areas of the Fe and MTM are also important to the growth process, because a low activity of CNT growth occurs for $N = 10$, leading to a tangled CNT morphology. Further characterization and control of the formation of nanocomposite catalyst layers could enable more unique architectures such as self-expanding "accordions" that give increased yield and height, which are difficult to obtain by other means. For example, by spatially varying the concentration of Fe throughout a LBL film, we may be able to induce stratification of the composite into more than two layers.

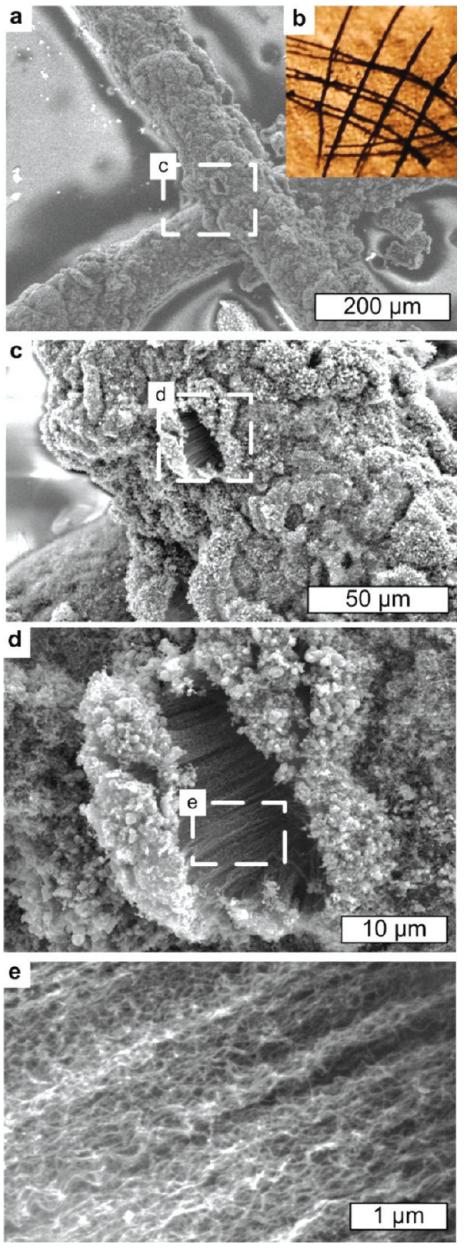

Figure 4. SEM images of CNT forests grown on Ti wire mesh with 10 support bilayers, showing conformal forest growth from the curved substrate at different magnifications in (a,b,c); and (d) anisotropic yet tortuous morphology of CNTs within the forest.

Conformal CNT Forest Growth on 3D Substrates. The versatility of the Fe-MTM system for CNT growth also enables growth of conformal CNT films on 3D substrates. Specifically, growth of CNTs on electrically conducting substrates could be used to directly build electrochemical devices and fluid filters; and growth of CNTs on advanced structural fibers could enable significant reinforcement of structural composites.

To this end, we deposited, annealed, and grew CNTs on a commercially available titanium (Ti) wire mesh (wire diameter $\approx$75 μm), and on aerospace-grade carbon fibers (diameter $\approx$10 μm, obtained from the Boeing Company). These results are shown in Figure 4 and Figure 5, respectively. On the Ti mesh, single-layer CNT forests grow radially from the surfaces of the individual wires including at the

(52) Manevitch, O. L.; Rutledge, G. C. *J. Phys. Chem. B* **2004**, *108*(4), 1428–1435.
(53) Meshot, E. R.; Hart, A. J. *Appl. Phys. Lett.* **2008**, *92*, 113107.

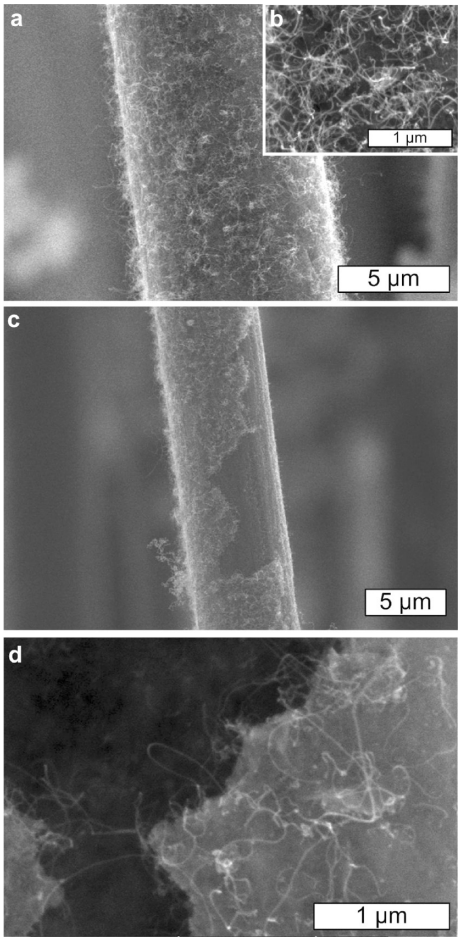

Figure 5. SEM images of CNT growth on carbon fibers by LBL deposition of supported catalyst: (a) segment of individual fiber with tangled CNT layer; (b) close-up image of tangled CNTs; (c) section of fiber where CNTs and support were partially delaminated; (d) close-up image showing contrast between support and fiber, indicating conformal coating of fiber by clay layers, and selectivity of CNT growth on support.

intersections of the mesh (Figure 4a−c). The radial and conformal morphology was confirmed by fracturing the wires as shown in Supporting Information, Figure S3. Localized extrusion of CNT ensembles is observed just like on the flat substrates, and local separation (Figure 4d) of the CNT bunches reveals the anisotropic texture of the forest (Figure 4e). The support remains on the substrate, indicating strong adhesion to the Ti wires, and amorphous carbon residue is observed on the top surface of the CNT forest.

CNTs grew conformally on the carbon fibers as well; however, the coating showed a sparse tangled morphology (Figure 5a−b), indicating a relatively low yield of CNTs compared to the other substrates. Therefore, we conclude that the activity of the nanocomposite catalyst is lower on carbon fibers than on the Si and Ti substrates. Because of the lower thermal stability of the carbon fibers in air, we could anneal the fibers at only 500 °C. We conclude this was insufficient to entirely oxidize the PDDA, because TGA of PDDA alone indicates that complete oxidation does not occur until above 600 °C. In this case, the remnant PDDA decreases the activity of the catalyst layer, and in turn decreases the CNT yield.

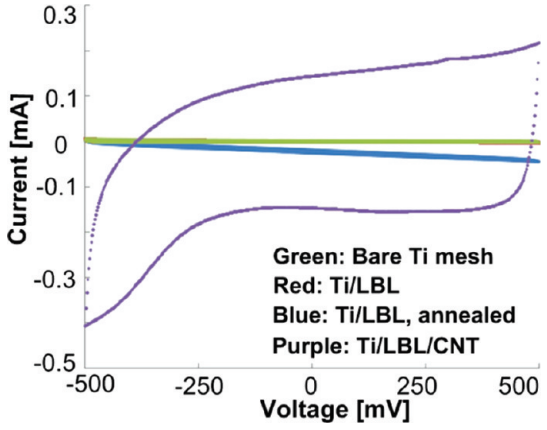

Figure 6. Cyclic voltammograms of CNT forests grown on Ti wire mesh substrates coated with $N = 40$ nanocomposite catalyst. The total capacitance of the CNT-coated mesh is 85-fold that of the bare substrate prior to deposition of the nanocomposite catalyst, annealing, and CNT growth. The data for the Ti (green curve) and Ti/LBL (red curve) samples overlap.

While it should be possible to achieve vertically aligned CNTs on carbon fibers, further work is required to process the nanocomposite layer to remove the PDDA at a sufficiently low temperature to prevent damage to carbon fibers. Likewise, it will be essential to evaluate how LBL deposition and thermal treatment could affect the electrical, thermal, and mechanical properties of the carbon fibers, which are essential for use in composites. Despite these present limitations, the conformal coating of such small fibers by our method, along with the robustness of the catalyst layers observed in our other experiments, indicates promise of this system to create CNT-tailored carbon fibers for composites.

Electrochemical Properties of CNTs Grown on 3D Substrates. The functionality of 3D CNT forests grown from nanocomposite catalysts was demonstrated by performing electrochemical measurements on the CNT-coated Ti mesh substrates. Four samples representing different stages within the catalyst assembly and CNT growth sequence were evaluated. The corresponding cyclic voltammograms for the 10th and last cycle of each measurement are shown in Figure 6. From this data, the capacitance (F), gravimetric capacitance (f), and capacitance per unit area (a) were calculated for each sample, and these values are given in Table 1. Derivation of these parameters is described in the Supporting Information.

We find that CNT coating results in an extreme enhancement of the electrochemical performance of the Ti mesh; specifically, the CNT-coated mesh has a specific capacitance of 0.44 F/g, which is 85-fold higher than the specific capacitance of the bare Ti mesh (5.1 mF/g). The specific capacitance of the CNTs alone is 7.56 F/g, which is approximately 1390 times higher than the bare mesh. This value is within a factor of 10 below benchmark values previously reported for CNTs transplanted onto electrically conducting substrates, where the fabrication process was designed specifically to maximize electrochemical storage.[54,55] The performance of our material may be limited by surface oxidation of the Ti mesh, by contact resistance at the CNT/MTM-Ti interface, and by the

Table 1. Electrochemical Performance of Ti Wire Mesh Samples, before and after CNT Growth[a]

	bare Ti mesh	Ti/LBL	Ti/LBL, annealed	Ti/LBL/CNT	CNTs only (calculated)
F [mF]	3.56×10^{-2}	4.16×10^{-2}	5.42×10^{-2}	2.94	2.89
f [F/g]	5.09×10^{-3}	7.55×10^{-3}	1.20×10^{-2}	**0.436**	**7.56**
a [m^2/g]	1.16×10^{-2}	2.20×10^{-2}	4.28×10^{-2}	1.11	19.3

[a] Each column is a different sample, and the performance of the CNTs alone was calculated using mass- and area-normalized values from the Ti/LBL/CNT and annealed Ti/LBL samples.

relatively low packing density (1.6%) of the CNTs. Nevertheless, the outstanding enhancement of capacitance demonstrates the versatility and potential of our growth method for decorating metal substrates with CNTs, while establishing an electrical path through CNTs within the nanocomposite catalyst layer. Additional efforts to characterize and optimize the catalyst-substrate interface, to tune the CNT growth characteristics to optimize trade-offs between density and ion transport, and to grow CNTs from nanocomposite catalysts on other metals, will enable further enhancements in energy storage properties.

Conclusion

We presented a versatile method for CNT growth in a substrate-independent fashion, using nanocomposite catalyst layers that are deposited by layer-by-layer assembly. By choosing the thickness of the MTM support layer, we demonstrate the ability to control the morphology of the CNT forest on flat substrates. Unique formation of self-stratified CNT forests by competition between Fe diffusion in MTM and the mechanical forces exerted by CNT self-organization indicates potential to create more complex CNT architectures by controlled self-assembly and diffusion of the catalyst components. The nanocomposite catalyst was further used to grow CNTs on metal meshes and aerospace-grade carbon fibers, and the conformal coating of these substrates with the MTM support layer demonstrates the ability to grow large areas of CNTs on 3D substrates. This technique can be extended to a wide variety of catalysts for CNT growth, and many new substrate configurations including large-area fabrics that will bolster development of nanostructured materials for applications including energy storage, advanced composites, and smart surfaces.

Acknowledgment. This work was supported by the University of Michigan Department of Mechanical Engineering, Department of Chemical Engineering, and College of Engineering. We thank Ming Qin for help making the MTM solutions; Sameh Tawfick, Michael Moebius for their assistance with SEM imaging and catalyst deposition; Davor Copic for assistance with CVD hardware and programming; Anne Juggernauth and Peter Ho for assistance with electrochemistry measurements and data analysis; and Arthur Woll, Eric Meshot, Erik Polsen and Michael Reinker for assistance with SAXS. We also thank Dr. Tom Tsotsis of the Boeing Company for providing carbon fiber samples. X-ray scattering was performed at the G1 beamline at the Cornell High-Energy Synchrotron Source (CHESS), which is supported by the National Science Foundation and the National Institutes of Health under Grant No. DMR-0225180.

Supporting Information Available: Calculation of electrochemical performance parameters, TGA data (Figure S1), additional SEM images of self-stratified CNT forests (Figure S2), and additional SEM images of CNT forests grown on Ti wire mesh substrates (Figure S3). This material is available free of charge via the Internet at http://pubs.acs.org.

(54) Futaba, D. N.; Hata, K.; Yamada, T.; Hiraoka, T.; Hayamizu, Y.; Kakudate, Y.; Tanaike, O.; Hatori, H.; Yumura, M.; Iijima, S. *Nat. Mater.* **2006**, *5*(12), 987–994.
(55) Du, C. S.; Pan, N. *J. Power Sources* **2006**, *160*(2), 1487–1494.